d'Collection

금속 나노와이어 기반 코어-쉘 구조 3차원 다공성 전극 개발

Synthesis of metal nanowire based core-shell structured 3D electrode with high porosity and electrical conductivity

2023년 2월

서울대학교 대학원

기계공학부

김 도 형

금속 나노와이어 기반 코어-쉘 구조 3차원 다공성 전극 개발

Synthesis of metal nanowire based core-shell structured 3D electrode with high porosity and electrical conductivity

지도교수 고 승 환

이 논문을 공학석사 학위논문으로 제출함

2022년 10월

서울대학교 대학원

기계공학부

김 도 형

김 도 형의 공학석사 학위논문을 인준함

2022년 12월

위 원 장 :   송 한 호   (인)

부위원장 :   고 승 환   (인)

위   원 :   도 형 록   (인)

Abstract

Three-dimensional (3D) porous electrodes with high conductivity, specific surface area, and material permeability have the potential to be applied in the fields of energy devices, catalysis, heat management, and sensors. In this report, we represent a novel solution process of synthesizing a 3D silver-gold core-shell structured nanowire foam electrode. The gold coated on the surface of the silver nanowires improves the chemical stability of the foam and nano-welds the junctions between nanowires to form a robust electrical path with structurally stable 3D nanowire percolation networks. This foam electrode has a high porosity and large pore size of 1–10 μm in a low-density region, thus exhibiting high hydraulic permeability similar to that of commercial carbon cloths. Finally, this research proposes a fabricating method for the composite of a foam electrode and a polyacrylamide hydrogel, in which the hydrogel networks are embedded in the electrode.

Table of contents

List of figures

Figure 1. The schematic diagrams of the AACNF fabrication process

Figure 2. The schematic diagrams of the hydraulic permeability test setup

Figure 3. (a) The morphology of the fabricated AACNF with different ethanol volume fractions. The weight ratio of the $HAuCl_4 \cdot 3H_2O$ against the sum of AgNWs and the $HAuCl_4 \cdot 3H_2O$ was 60% and the weight percent of the AgNWs was 0.15. (b) The volume of fabricated AACNF against the precursor solutions (left axis) and density of the fabricated AACNF (right axis) with respect to the ethanol volume fraction. The error bars are the standard deviation (s.d.) for $N = 3$ samples.

Figure 4. (a) The morphology of the fabricated AACNF with respect to the weight ratio of the $HAuCl_4 \cdot 3H_2O$ against the sum of AgNWs and the $HAuCl_4 \cdot 3H_2O$. The ethanol volume fraction was 0.2 and the weight percent of the AgNWs was 0.25. (b) ICP-MS analysis of the released Ag ions from AACNF with different $HAuCl_4 \cdot 3H_2O$ concentrations after treatment of 2 M H_2O_2 for 30 min. ND, not detected.

Figure 5. The morphology of the fabricated AACNF with respect to the weight percent of AgNWs. The ethanol volume fraction was 0.2 and the weight ratio of the $HAuCl_4 \cdot 3H_2O$ against the sum of AgNWs and the $HAuCl_4 \cdot 3H_2O$ was 60%.

Figure 6. (a) An SEM image of the lyophilized AACNF. (b) Electrical conductivity (left axis) and density (right axis) of the AACNF with respect to the weight percent of AgNWs. The error bars are the s.d. for $N = 3$ samples.

Figure 7. Hydraulic permeability of the AACNF with varying weight percent of

AgNWs from 0.25 to 2.0. The error bars are the s.d. for $N = 5$ samples.

Figure 8. (a) The schematic diagrams of the AACNF/PAAm hydrogel composite fabrication process and (b) an optic image of the stretched AACNF/PAAm hydrogel composite.

Figure 9. (a) Electrical conductivity of AACNF, AACNF/PAAm hydrogel composite, and the PAAm hydrogel with AgNWs against the weight percent of the AgNWs. The error bars are the s.d. for $N = 3$ samples. (b) Relative resistance with respect to the strain applied to the AACNF/PAAm hydrogel composite at varying densities of AACNF. (c) Cyclic loading and unloading test (50% tensile strain, 12 s cycle^{-1}) to the AACNF/PAAm hydrogel composite. (d) Relative resistance of the AACNF/PAAm hydrogel composite with repeated swelling and deswelling test.

Chapter 1. Introduction

1.1. Study backgrounds

The three-dimensional (3D) porous electrode has been used in broad fields such as fuel cells[1], supercapacitors[2], catalysis, thermal management system[3], and sensors[4] due to its unique features; high conductivity, specific surface area, and material permeability. Especially, metal nanowire-based aerogels synthesized by freeze-drying[5], critical point drying[6], and freeze-casting[7] have been recently studied. These aerogels are ultralight, highly porous, and highly conductive. However, these aerogels would suffer from oxidation as they are based on silver nanowires (AgNWs) or copper nanowires.

On the other hand, there have been studies of synthesizing gold-silver (Au-Ag) core-shell nanowires[8, 9]. They have the advantages of both AgNWs and Au shells, which have high electrical conductivity, high aspect ratio, and chemical stability. To synthesize Au-Ag core-shell nanowires, additional processes of coating Au on the AgNWs and purification were required.

1.2. Purpose of this research

In this study, we introduce a one-step fabrication method for 3D Ag-Au core-shell structured nanowire foam (AACNF) with high electrical conductivity, porosity, hydraulic permeability, and chemical stability. The fabrication involves mixing three solutions: the Ag preparation solution, the Au precursor, and ethanol. The reduction of Au cations by L-ascorbic acid (L-AA) on the surface of pristine AgNWs results in the formation of a 3D percolation networks and gold coating on

the AgNWs surface, as well as nano-welding between the AgNWs. The optimization of the AACNF fabrication process was performed by considering three parameters: the ethanol fraction in the AACNF precursor solutions, the Ag: Au ratio, and the concentration of the AACNF precursor solutions. The high porosity and permeability of the AACNF enable the formation of an AACNF/polyacrylamide (PAAm) hydrogel composite, which has excellent stretchability and maintains its electrical conductivity under external strain.
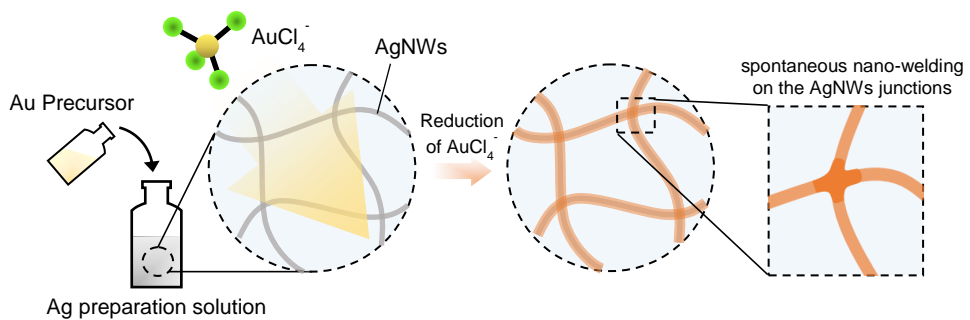

Figure 1. The schematic diagrams of the AACNF fabrication process

Chapter 2. Methods

2.1. Materials

Polyvinylpyrrolidone (PVP, Mw = 360,000, Mw = 40,000), Copper(II) chloride dihydrate (CuCl$_2$·2H$_2$O, 99.999%) Gold(III) chloride trihydrate (HAuCl$_4$·3H$_2$O, $\geq$ 99.9% trace metals basis), sodium sulfite (Na$_2$SO$_3$, ACS reagent, $\geq$98.0%), L-AA (ACS reagent, $\geq$99%), Acrylamide (AAm, suitable for electrophoresis, $\geq$99%), and N,N′-methylenebis(acrylamide) (MBA, powder, for molecular biology, suitable for electrophoresis, $\geq$99.5%) were purchased from Sigma Aldrich. Ethylene glycol (EG, 99.5%), sodium hydroxide (NaOH, bead, 98%), and Ammonium persulfate (APS, 98%) were purchased from Samchun Chemical Co., Ltd. Silver(I) nitrate (AgNO$_3$, 99.9%) was purchased from Kojima Co., Ltd.

2.2. Synthesis of the AgNWs

A polyol-mediated method that was modified from a previous study was used to synthesize the AgNWs[10]. 260 mL of EG with 3.182 g of PVP (Mw = 360,000) were preheated to 175 ℃. 1.6 mL of 4 mM CuCl$_2$·2H$_2$O was added once the temperature had reached its saturation point. After 10 min, 60 mL of 98 mM AgNO$_3$ in EG are injected at the rate of 180 mL h^{-1}. After the injection is complete, we stop stirring and wait for the synthesis reaction for an additional 2 h. As-prepared AgNWs were diluted with acetone (5 times by volume) and the remaining solution was flushed away to get aggregated nanowires. Aggregated nanowires were redispersed in water and repeatedly cleaned with 2500 rpm centrifugation for 10 min. The purified AgNWs solution is then adjusted to a concentration of 15.875 mg mL^{-1}.

2.3. Preparation of the AACNF

This recipe is for the AACNF with 0.25 wt% of AgNWs and 0.2 volume fraction of ethanol. We synthesized Au precursor by mixing 0.095 M of $HAuCl_4 \cdot 3H_2O$ and 1 M of NaOH in a volume ratio of 1:1, and then mixing this mixture with 0.15 M of Na_2SO_3 in a volume ratio of 1:1. Then, we left Au precursor at room temperature undisturbed for 2 h. Additionally, We synthesized the Ag preparation solution by orderly combining AgNWs (15.875 mg mL^{-1}), PVP (Mw 40,000; 7.2 wt%), 1.12 M of NaOH, 1.12 M of L-AA and 0.07 M of Na_2SO_3 by a volume ratio of 16:10:5:5:4. Finally, the 2:2:1 volume ratio of Au precursor, Ag preparation solution and ethanol were mixed and kept undisturbed at room temperature for 1 h.

2.4. Hydraulic permeability test

We measured the hydraulic permeability, a viscous permeability of the water passing through the AACNF, by inserting AACNF like a filter into the manufactured chamber and passing a certain flux of water (0.0212, 0.0424, 0.0636, 0.0849, 0.1061, 0.1273, 0.1485, 0.1698, 0.1910, 0.2122 mm s^{-1}) by a motor pump (**Figure 2**). Then, the hydraulic permeability could be calculated by substituting the pressure drop of water, obtained through the height of the water level rise, into the equation of Darcy's law below

$$q = -k\Delta P/(\mu L)$$

where q is the flux of water passing through the AACNF, k is the hydraulic permeability of the AACNF, μ is the dynamic viscosity of the water, and ΔP is the pressure drop over L which is a given distance along AACNF.
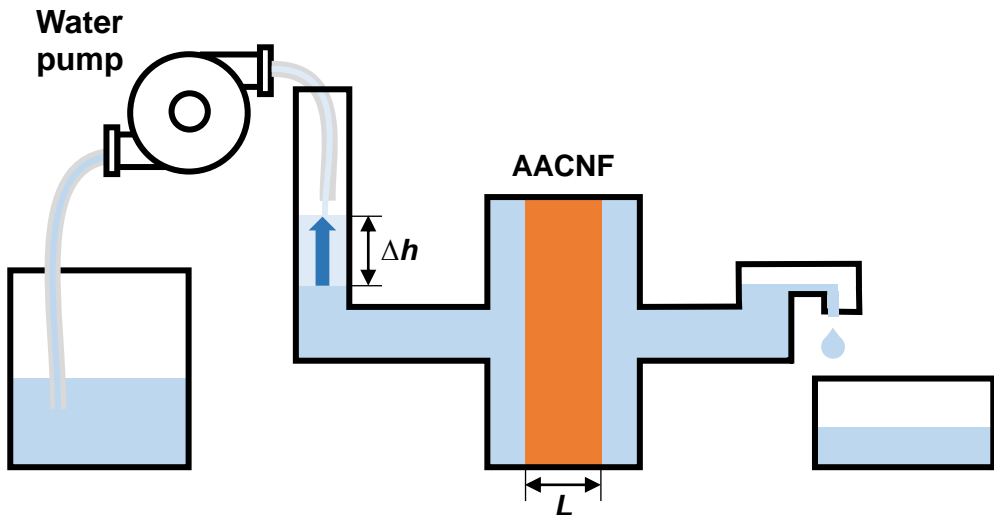
Figure 2. The schematic diagrams of the hydraulic permeability test setup

2.5. Preparation of the AACNF/PAAm hydrogel composite

A PAAm hydrogel precursor solution was synthesized by dissolving 18 wt% of AAm as a monomer, 0.0128 wt% of MBA as a crosslinker, and 0.082 wt% of APS as an initiator. Then, The existing solution inside the AACNF was gently replaced with the PAAm hydrogel precursor solution. The resulting PAAm hydrogel solution within the AACNF was thermally polymerized at 60°C for 3 h.

Chapter 3. Optimizing the AACNF fabrication process

3.1. The effect of the Ethanol fraction

Adding ethanol to the AACNF precursor solutions can lower the required density for forming 3D AgNW percolation networks. This outcome is a result of the alteration in the morphology of the PVP ligands in different solvents, as well as the preferential adsorption of ethanol to the PVP ligands. The solubility of PVP in the solvent impacts its morphology, where it collapses in water, but expands in ethanol, which is a good solvent for PVP[11]. The expanded PVP ligands of AgNWs in ethanol-rich solutions could facilitate the adsorption of Au cations on the surface of AgNWs, thus enhancing the formation of gold coatings and nano-welds at the AgNWs junctions. Furthermore, the PVP ligands of AgNWs exhibit a higher affinity for ethanol than water when the ethanol molar fraction is below 0.5[12]. This leads to the formation of ethanol shells on the AgNWs surface, which, upon merging, create an ethanol-rich domain around the AgNW networks. As the ethanol volume fraction of the AACNF precursor solutions increases, the ethanol-rich domain becomes lighter and tends to rise to the water-air interface, facilitating the synthesis of a mold-fitted AACNF without sinking by gravity(**Figure 3a**, v/v = 0.2). However, if the ethanol volume fraction exceeds the optimal point, the ethanol-rich domain rises too strongly, resulting in AACNF formation at the water-air interface (**Figure 3a**, v/v = 0.3, 0.4).
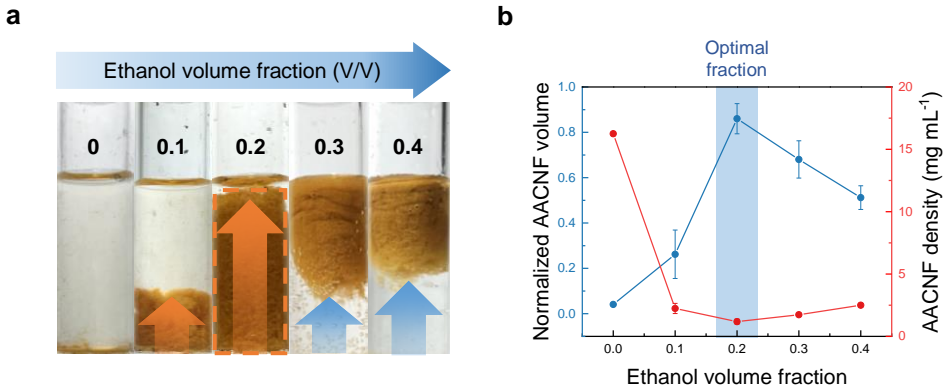
Figure 3. (a) The morphology of the fabricated AACNF with different ethanol volume fractions. The weight ratio of the $HAuCl_4 \cdot 3H_2O$ against the sum of AgNWs and the $HAuCl_4 \cdot 3H_2O$ was 60% and the weight percent of the AgNWs was 0.15. (b) The volume of fabricated AACNF against the precursor solutions (left axis) and density of the fabricated AACNF (right axis) with respect to the ethanol volume fraction. The error bars are the standard deviation (s.d.) for $N = 3$ samples.

3.2. The effect of the Ag: Au ratio

The proportion of Au cation to the AgNWs is crucial for forming a mold-fitted, chemically stable AACNF. Insufficient Au cation leads to a collapse of the AACNF structure, yet increasing the proportion of Au cation results in a mold-fitted and structurally stable AACNF with sufficient gold coating and nano-welded junctions (**Figure 4a**). An inductively coupled plasma mass spectrometry (ICP-MS) analysis was conducted to measure the degree of gold coating on AACNF after a 30 min treatment with 2 M H_2O_2 (**Figure 4b**). Results showed that chemically stable and mold-fitted AACNF can be synthesized with a ratio of 60 wt% or higher of ($HAuCl_4 \cdot 3H_2O$) / (AgNWs + $HAuCl_4 \cdot 3H_2O$).
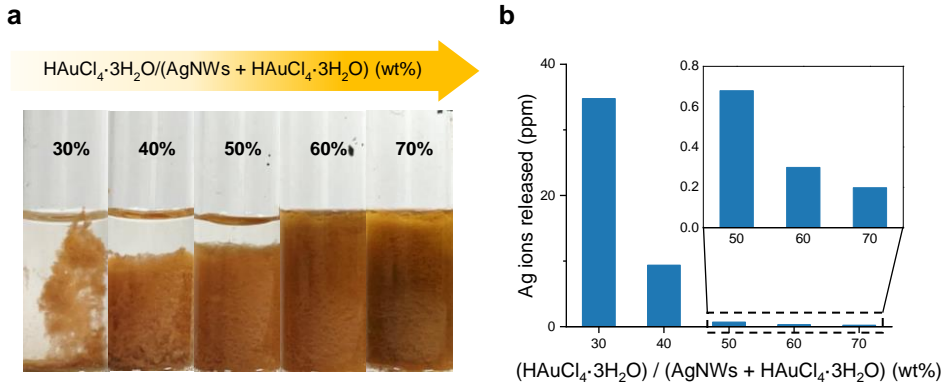
Figure 4. (a) The morphology of the fabricated AACNF with respect to the weight ratio of the $HAuCl_4 \cdot 3H_2O$ against the sum of AgNWs and the $HAuCl_4 \cdot 3H_2O$. The ethanol volume fraction was 0.2 and the weight percent of the AgNWs was 0.25. (b) ICP-MS analysis of the released Ag ions from AACNF with different $HAuCl_4 \cdot 3H_2O$ concentrations after treatment of 2 M H_2O_2 for 30 min. ND, not detected.

3.3. The effect of the AACNF precursor concentration

Following the attainment of the two previously discussed criteria, the synthesis of AACNF was conducted by altering the concentration of its precursor. As the solute density increased, the formation of 3D nanowire percolation networks was observed, leading to the establishment of a bulk structure of AACNF. The increment in junctions also enhanced the stability of the nanowire networks' structure, thereby augmenting the resistance of AACNF against collapse. The threshold for the formation of mold-fitted AACNF was determined to be 0.15 weight percent of AgNWs, which resulted in the synthesis of a highly porous and lightweight foam electrode (**Figure 5**).
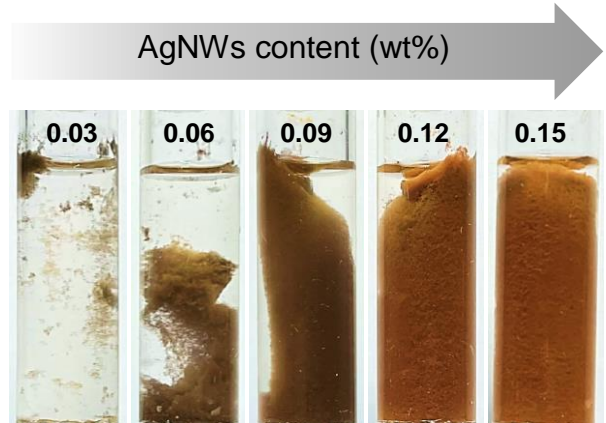
**Figure 5.** The morphology of the fabricated AACNF with respect to the weight percent of AgNWs. The ethanol volume fraction was 0.2 and the weight ratio of the $HAuCl_4 \cdot 3H_2O$ against the sum of AgNWs and the $HAuCl_4 \cdot 3H_2O$ was 60%.

Chapter 4. Results

4.1. Material characterizations
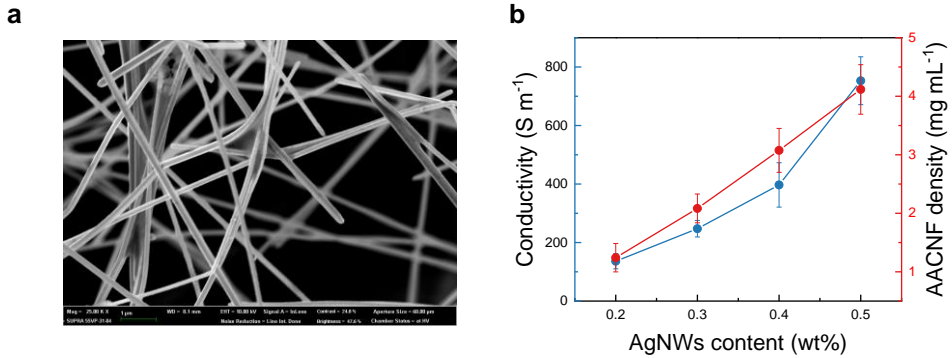
Figure 6. (a) An SEM image of the lyophilized AACNF. (b) Electrical conductivity (left axis) and density (right axis) of the AACNF with respect to the weight percent of AgNWs. The error bars are the s.d. for $N = 3$ samples.

Figure 6a shows A scanning electron microscopy (SEM) image of lyophilized AACNF. It reveals the nanowires to be intricately woven in a manner reminiscent of spider webs and exhibiting a highly porous nature. The pores of AACNF have a size distribution of approximately 1-10 μm, thereby making them capable of accommodating a multitude of under 10 μm size materials. The junctions between the nanowires are supported by nano-welded Au parts, which could contribute to the formation of electrical paths within the percolation networks and serve to maintain the stability of the overall structure of the AACNF. As the density of AACNF increases, the number of electrical paths passing through the nanowire junctions also increases, resulting in a monotonic rise in both density and electrical conductivity, from 1.24 to 4.12 mg mL^{-1} and 136.21 to 753.04 S m^{-1}, respectively, as depicted in **Figure 6b**.

4.2. Hydraulic permeability of the AACNF
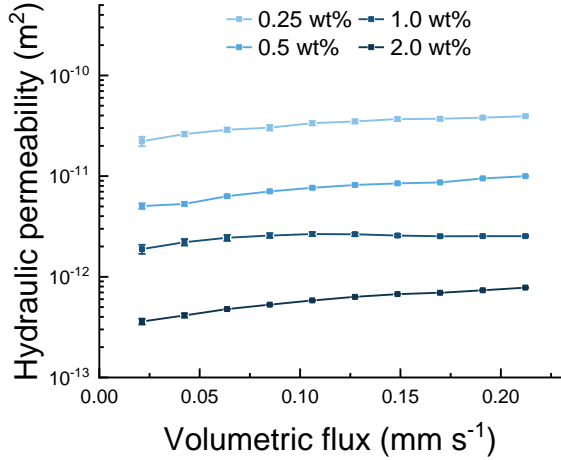
Figure 7. Hydraulic permeability of the AACNF with varying weight percent of AgNWs from 0.25 to 2.0. The error bars are the s.d. for $N = 5$ samples.

The experimentally determined viscous permeability of water flowing through AACNF of varying density is depicted in **Figure 7**. This hydraulic permeability is calculated based on Darcy's law and ranges from 7.81×10^{-13} to 3.93×10^{-11} m^2 at a volumetric flux of 0.2122 mm s^{-1} for AACNF densities from 0.25 to 2.0 wt% of AgNWs. As the density of AACNF increases, the nanowire networks become denser, decreasing porosity and pore size, thus hindering water flow. The low-density AACNF has a hydraulic permeability of 3.93×10^{-11} m^2, comparable to commercially available porous carbon cloth with permeabilities about 1×10^{-11} to 1×10^{-10} m^2, thereby enabling effective permeation of materials through the pores of AACNF[13]. It should be noted that while the electrical conductivity and structural stability of AACNF improve with density, the hydraulic permeability and pore size decrease. This issue can be addressed by adjusting the AACNF precursor concentration depending on the requirements.

## 4.3. Characterization of the AACNF/PAAm hydrogel composite
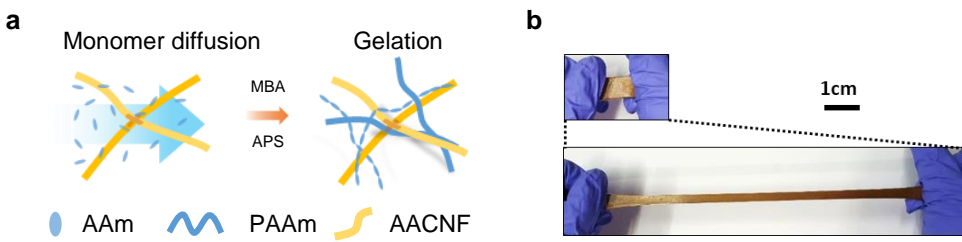
Figure 8. (a) The schematic diagrams of the AACNF/PAAm hydrogel composite fabrication process. (b) An optic image of the stretched AACNF/PAAm hydrogel composite.

Due to its highly porous nature, AACNF could contain heterogeneous materials and form a hierarchical structure. A hydrogel polymer chain matrix could be a good candidate. We diffuse hydrogel monomers (AAm), crosslinkers (MBA), and initiators (APS) inside the pore of the AACNF and then thermally polymerized it to synthesize a hierarchical structure of PAAm hydrogel with AACNF (**Figure 8a**). **Figure 8b** shows that PAAm hydrogel is well embedded inside the AACNF to form a complete composite. The AACNF/PAAm hydrogel composite exhibits great elasticity capable of withstanding tensile deformation of 700% or more, which is the intrinsic property of the hydrogel.

As the nano-welded junctions between nanowires ensure the robustness of the electrical paths, the electrical conductivity decrease before and after the hydrogel gelation inside the AACNF is small, about 7.26 to 14.93% (**Figure 9a**). On the other hand, a simple composite with AgNWs as conducting fillers of PAAm hydrogel has a low electrical conductivity of about 1.66×10^{-5} to 6.49×10^{-5} times that of AACNF/PAAm hydrogel composite due to the relatively poor contact

between nanowires.

 Furthermore, We investigated the changes in electrical conductivity under the external tensile strain of the AACNF/PAAm hydrogel composite according to the density of AACNF (**Figure 9b**). As the density of the AACNF increased to the optimal point (0.2 wt% to 0.4 wt% of the AgNWs), the electrical conductivity change of the composite with external tensile strain decreases as the junctions of the nanowire networks increased. However, if the density of the AACNF increases beyond the optimum point, the electrical conductivity retention of the composite to the tensile strain is weakened (**Figure 9b,** 0.5 wt% of AgNWs). We hypothesized that the reason for this phenomenon was that the materials for PAAm hydrogel could not be uniformly dispersed at a density of AACNF above the optimum point (The techniques and conditions used for permeating the hydrogel precursor into the AACNF were consistent), resulting in phase separation between the AACNF and the hydrogel networks, which leads to the crack of conductive paths in a tensile state. In addition, AACNF/PAAm hydrogel composite demonstrated stable electrical conductivity during repeated cycles of external strain loading and unloading, as well as the isotropic swelling and deswelling behavior of the hydrogel (**Figure 9c, d**).
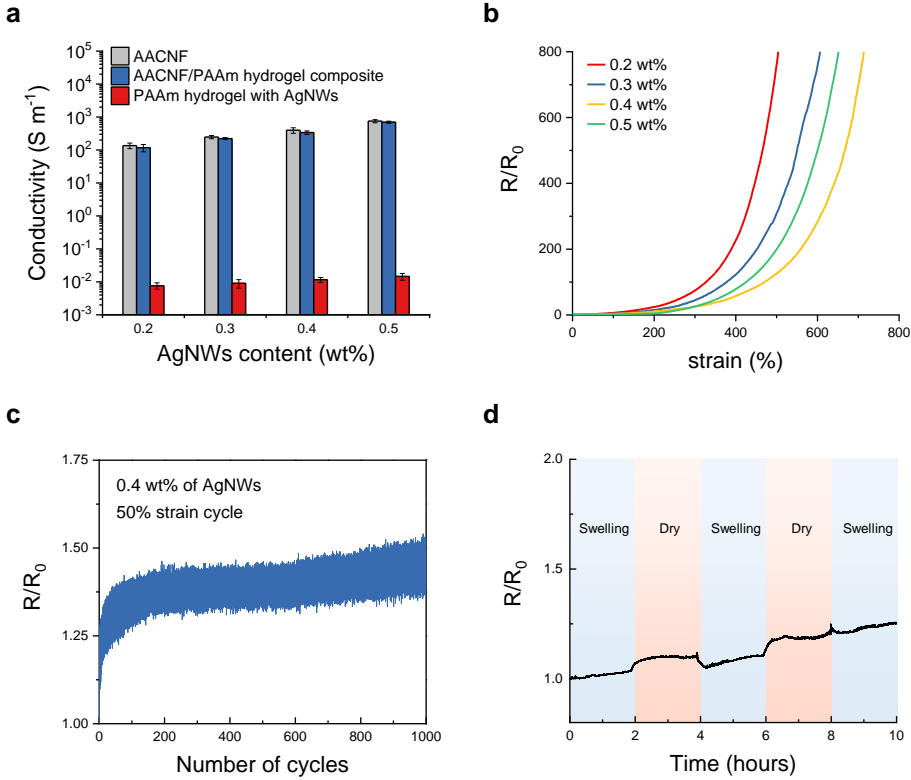
Figure 9. (a) Electrical conductivity of AACNF, AACNF/PAAm hydrogel composite, and the PAAm hydrogel with AgNWs against the weight percent of the AgNWs. The error bars are the s.d. for $N = 3$ samples. (b) Relative resistance with respect to the strain applied to the AACNF/PAAm hydrogel composite at varying densities of AACNF. (c) Cyclic loading and unloading test (50% tensile strain, 12 s cycle[-1]) to the AACNF/PAAm hydrogel composite. (d) Relative resistance of the AACNF/PAAm hydrogel composite with repeated swelling and deswelling test.

Chapter 5. Conclusion

5.1. Summary of this work

In this paper, a nanowire-based Ag-Au core-shell structured 3D electrode with high porosity was fabricated by a simple one-step solution process. It was simply fabricated by mixing the Ag preparation solution, Au precursor, and ethanol. As au cations are reduced on the AgNWs surfaces, simultaneous nano-welding occurs on the junctions between AgNWs. Because of its nano-welded junctions, it could maintain its structure with robust electrical paths at 3D percolation networks of nanowires. It had high electrical conductivity and ultralow density which were tunable by changing the concentration of AgNWs and other materials. Due to the AACNF's high porosity and pore size of 1-10 μm, its hydraulic permeability was high as commercial carbon clothes. In addition, we could form a hierarchical structure of AACNF and PAAm hydrogel by diffusing hydrogel monomers, crosslinkers, and initiators inside the AACNF and then polymerizing it. This composite had high elasticity, an inherent property of the hydrogel, and an electrical conductivity as high as pristine AACNF.

5.2. Future work

This study evaluated the high electrical conductivity and porosity of the AACNF, as well as its large specific surface area, which is achieved through 3D nanowire networks. In particular, the high permeability of AACNF would ensure facile material transfer to the electrode surface. These features show the potential of AACNF to be applied to the fields of energy devices. Additionally, due to its

chemical stability, AACNF could also be utilized in the field of bioelectronics, or even in harsh conditions.

Besides these unique features, AACNF has tunable density, porosity, and pore size. Thus, if we want to diffuse some materials under 1-10 μm, we could tune the density of the AACNF regarding the size of the materials and then diffuse those materials. We fabricated a hierarchical composite of AACNF and hydrogel networks using this property. This soft electrode has the potential to be applied to various fields such as soft sensors, actuators, and bioelectronics. Furthermore, we expect that novel heterogeneous structures would be created by embedding various materials inside the AACNF like polymer networks, micro/nanoparticles, and cells.

Reference

1.   Steele, B. C.; Heinzel, A., Materials for fuel-cell technologies. *Nature* **2001,** *414* (6861), 345-352.

2.   Yu, Z.;   Tetard, L.;   Zhai, L.; Thomas, J., Supercapacitor electrode materials: nanostructures from 0 to 3 dimensions. *Energy & Environmental Science* **2015,** *8* (3), 702-730.

3.   Li, W.;   Qu, Z.;   He, Y.; Tao, Y., Experimental study of a passive thermal management system for high-powered lithium ion batteries using porous metal foam saturated with phase change materials. *Journal of power sources* **2014,** *255*, 9-15.

4.   Ha, K. H.;   Zhang, W.;   Jang, H.;   Kang, S.;   Wang, L.;   Tan, P.; Hwang, H.; Lu, N., Highly sensitive capacitive pressure sensors over a wide pressure range enabled by the hybrid responses of a highly porous nanocomposite. *Advanced Materials* **2021,** *33* (48), 2103320.

5.   Tang, Y.;   Gong, S.;   Chen, Y.;   Yap, L. W.; Cheng, W., Manufacturable conducting rubber ambers and stretchable conductors from copper nanowire aerogel monoliths. *ACS nano* **2014,** *8* (6), 5707-5714.

6.   Jung, S. M.;   Preston, D. J.;   Jung, H. Y.;   Deng, Z.;   Wang, E. N.; Kong, J., Porous Cu nanowire aerosponges from one-step assembly and their applications in heat dissipation. *Advanced Materials* **2016,** *28* (7), 1413-1419.

7.   Qian, F.;   Lan, P. C.;   Freyman, M. C.;   Chen, W.;   Kou, T.;   Olson, T. Y.;   Zhu, C.;   Worsley, M. A.;   Duoss, E. B.;   Spadaccini, C. M.;   Baumann, T.; Han, T. Y.-J., Ultralight Conductive Silver Nanowire Aerogels. *Nano Letters* **2017,** *17* (12), 7171-7176.

8.   Lee, H.;   Hong, S.;   Lee, J.;   Suh, Y. D.;   Kwon, J.;   Moon, H.; Kim, H.;   Yeo, J.; Ko, S. H., Highly stretchable and transparent supercapacitor by Ag–Au core–shell nanowire networks with high electrochemical stability. *ACS Applied Materials & Interfaces* **2016,** *8* (24), 15449-15458.

9.   Choi, S.;   Han, S. I.;   Jung, D.;   Hwang, H. J.;   Lim, C.;   Bae, S.; Park, O. K.;   Tschabrunn, C. M.;   Lee, M.;   Bae, S. Y.;   Yu, J. W.;   Ryu, J. H.; Lee, S. W.;   Park, K.;   Kang, P. M.;   Lee, W. B.;   Nezafat, R.;   Hyeon, T.; Kim, D. H., Highly conductive, stretchable and biocompatible Ag-Au core-sheath

nanowire composite for wearable and implantable bioelectronics. *Nat Nanotechnol* **2018,** *13* (11), 1048-1056.

10.   Andrés, L. J.;   Menéndez, M. F.;   Gómez, D.;   Martínez, A. L.;   Bristow, N.;   Kettle, J. P.;   Menéndez, A.; Ruiz, B., Rapid synthesis of ultra-long silver nanowires for tailor-made transparent conductive electrodes: proof of concept in organic solar cells. *Nanotechnology* **2015,** *26* (26), 265201.

11.   Yang, T.-H.;   Ahn, J.;   Shi, S.; Qin, D., Understanding the Role of Poly(vinylpyrrolidone) in Stabilizing and Capping Colloidal Silver Nanocrystals. *ACS Nano* **2021,** *15* (9), 14242-14252.

12.   Guettari, M.;   Belaidi, A.;   Abel, S.; Tajouri, T., Polyvinylpyrrolidone behavior in water/ethanol mixed solvents: comparison of modeling predictions with experimental results. *Journal of Solution Chemistry* **2017,** *46* (7), 1404-1417.

13.   Wong, A. A.; Aziz, M. J., Method for comparing porous carbon electrode performance in redox flow batteries. *Journal of The Electrochemical Society* **2020,** *167* (11), 110542.

국문 초록

금속 나노와이어 기반 코어−쉘 구조
3차원 다공성 전극 개발

김도형

기계공학부

서울대학교 대학원

높은 전도성, 비표면적 및 재료 투과성을 갖는 3차원(3D) 다공성 전극은 에너지 소자, 촉매, 열 관리 및 센서 분야에 활용되어 왔다. 본 연구에서는, 3D 은-금 코어-쉘 구조 나노와이어 다공성 전극을 합성하는 새로운 용액 공정 방법을 제시한다. 은 나노와이어 표면에 코팅된 금은 화학적 안정성을 향상시키며, 나노와이어 접합부를 나노-용접함으로써 구조적으로 안정한 3D 나노와이어 퍼콜레이션 네트워크와 견실한 전기전도 경로를 형성한다. 본 다공성 전극은 1–10 μm의 큰 공극 크기와 높은 공극률을 가지며, 저밀도 영역에서 상용 Carbon clothes와 유사한 정도의 높은 투수율을 보인다. 최종적으로, 본 연구에서는 폴리아크릴아마이드 하이드로겔 네트워크를 다공성 전극에 내장한 계층 구조의 복합체 제조 방법을 제시한다.

주요어 : 삼차원 전극, 다공성 전극, 코어-쉘 구조, 금속 나노와이어, 물질 전달, 계층 구조

학 번 : 2021-29792